

Full length article



Light-induced enhanced torque on double-V-type quantum emitters via quantum interference in spontaneous emission

Hamid R. Hamed^{a,*}, Julius Ruseckas^a, Vassilios Yannopoulos^b, Dimitrios Karaoulanis^c, Emmanuel Paspalakis^d

^a Baltic Institute of Advanced Technology, LT-01403, Pilies St. 16-8 Vilnius, Lithuania

^b Department of Physics, School of Applied Mathematical and Physical Sciences, National Technical University of Athens, Athens 157 80, Greece

^c Department of Electromagnetics, Electrooptics and Electronic Materials, School of Electrical and Computer Engineering, National Technical University of Athens, 15780 Athens, Greece

^d Materials Science Department, School of Natural Sciences, University of Patras, Patras 265 04, Greece

ARTICLE INFO

Keywords:

Quantum interference in spontaneous emission
Double-V-type quantum system
Light-induced enhanced torque
Bismuth-chalcogenide

ABSTRACT

We consider interaction of a pair of counterpropagating spatially inhomogeneous weak vortex beams with a quantum emitter that has a double-V level scheme and closely situated upper levels. We show that in such a situation a quantized torque is exerted on the emitter, which is directly proportional to the topological charge of the vortices and is strongly influenced and even enhanced by the quantum interference of spontaneous emission from the doublet. Depending on the particular initial states of the emitter, absorption, optical transparency, or lasing without inversion can be realized. The interference in spontaneous emission can be modified when the double-V emitter is situated above the surface of a thick slab of Bi₂Te₃ and the vortex beams propagate parallel to the surface. The light-induced torque rotates the emitters generating a persistent toroidal current flow above the bismuth-chalcogenide surface, whose intensity is remotely controlled by the distance from the surface.

1. Introduction

The interaction of laser pulses with quantum matter has revealed various interesting phenomena, such as electromagnetically induced transparency (EIT) [1–3], coherent population trapping (CPT) [4–6], stimulated Raman adiabatic passage (STIRAP) [7,8], lasing without inversion (LWI) [9,10], and others. These coherent optical phenomena have various applications such as slow light [11,12], enhanced non-linear optics [13,14], storage of quantum information [15] and optical switching [16].

Light beams with spiral phase dislocations can carry an orbital angular momentum (OAM) arising from its phase cross-section [17,18]. A spiral phase $e^{il\phi}$ linearly proportional to the azimuthal angle ϕ is associated with a null field at the center. The OAM carried by the light beam is discretized with the integer number l . This number, known as the topological charge or order of the beam, characterizes the number of times the beam makes the azimuthal 2π phase shifts [17]. The phase singularity at the core of the beam evolves its ring-shaped intensity profile. Such optical vortices with phase singularities have been generated [19], and are routinely created so as to carry specific values of OAM [20].

Interaction of optical vortices with matter leads to a number of interesting effects [21–28]. Among them, there has been a great deal of interest on the mechanical effects of OAM on particles and atoms [29]. Light beams with OAM have been employed to rotate particles held in optical tweezers [30,31]. Transfer of the OAM to matter has been shown to generate a torque associated with the transfer of wave energy [32–35]. Coherent transfer of the OAM of a photon to a Bose-Einstein condensate (BEC) of sodium atoms using a two-photon stimulated Raman process with Laguerre–Gaussian (LG) beams has been demonstrated by Andersen et al. [34]. Counter-propagating LG and Gaussian laser beams, with the same linear polarization, have been applied to the BEC, allowing to trap the atoms axially. The OAM of LG beam imparts then a torque on the center of mass of each trapped atom and rotates the medium about the beam axis, generating an atomic vortex state. In another work, Lembessis and Babiker proposed a different scenario to induce torque on an atomic three-level Λ BEC gas interacting with two counter-propagating spatially-dependent beams, generating a current flow [36]. This torque has a rotating effect on the whole BEC as the many-body wave function of the BEC can be

* Corresponding author.

E-mail addresses: hamid.hamed@tfai.vu.lt (H.R. Hamed), julius.ruseckas@bpti.eu (J. Ruseckas), paspalak@upatras.gr (V. Yannopoulos), vyannop@mail.ntua.gr (E. Paspalakis).

<https://doi.org/10.1016/j.optlastec.2023.109550>

Received 7 February 2023; Received in revised form 7 April 2023; Accepted 26 April 2023

0030-3992/© 2023 Elsevier Ltd. All rights reserved.

well approximated by the product of identical single-particle wave functions [34].

There are many motivations to explore the characteristics of the induced torque imposed by the light interacting with different matter-light coupling schemes, most of which are related to the applications. The induced torque imparted on quantum emitters (QEs) [atoms, molecules, and quantum dots] is very important in particular experiments in order to characterize the dynamics of the ensemble, and possesses potential applications in the realization of superconducting atomic devices, generating superflow and superposition of macroscopic states in atomic vapors [37], and in quantum repeaters where the flying qubits are photons carrying an OAM [38].

Here we explore a novel scheme to control and even enhance the light induced torque on quantum emitters: that of quantum interference (QI) of spontaneous emission channels. Although the three-level V-type scheme is the most often considered in literature to exhibit QI in spontaneous emission [39–48], this study considers a rather more complicated QE in the form of a double-V light-matter coupling with four energy levels consisting of two linked V-type subsystems. In the V-type QE, the QI of the spontaneous emission channels takes place only if two closely lying upper levels decay to the common lower level [40,41]. This requires the corresponding electric dipoles for the spontaneous emission process to be nonorthogonal, and as a result the interference can be maximized for almost parallel (anti-parallel) orientations of the corresponding dipoles. However, a perfect quantum interference (i.e., $p = 1$ where p is the degree of QI) cannot happen if each leg of the V-model system interacts with an individual coupling field [41], as in this case both Rabi frequencies of laser fields coupling each transition are connected to the alignment of the two matrix elements such that Rabi-frequencies reduce to zero if the QI is perfect. The situation is different in the four-level double-V light-matter coupling scheme with two upper states and two lower states, allowing the perfect interference $p = 1$ with individual coupling. In such a system, the two excited states are coupled to a third lower level with two laser beams, while they decay to a fourth lower level allowing the corresponding spontaneous-emission channels to interfere.

We start first with the effects of QI from spontaneous emission on the control of light-induced torque and generation of current flow in such a double-V QE. We derive the basic expressions describing the quantized torque imposed by spatially inhomogeneous laser beams on the center of mass of the individual double-V-model emitters. The torque imparted on the center of mass of each trapped QE can rotate an ensemble of such QEs about the beam axis, creating a toroidal trap. Compared to the earlier schemes [36,49], the induced torque here is strongly dependent on the initial internal state of the QEs, and can be well controlled and even enhanced by the degree of QI from spontaneous emission channels, providing a new degree of freedom on manipulating the torque and the resulting ring-shaped current flow.

Since the usual situation in QEs provides orthogonal dipole matrix elements, therefore the QI in spontaneous emission cannot take place. It has been demonstrated by Agarwal that the QI can be simulated by placing the QE in close proximity to a photonic structure that creates anisotropic Purcell effect and suppresses strongly (ideally completely) the decay rate for one the two possible dipole orientations, while retaining the decay rate for the second orientation [50]. The idea has been utilized in a variety of photonic structures, examples include negative periodic dielectric structures [45], refractive index metamaterials and their structures [42,46,51], hyperbolic metamaterials [47], semiconductor microcavities [48], metallic and metal-dielectric nanostructures [52,53], and two-dimensional materials [54–56].

Using this fact, in the second step of this study we investigate the light-induced torque in the double-V QE when it is placed close to a new class of materials for creating QI, i.e., a bismuth chalcogenide (a Bi_2Te_3 specimen in the form of a simple geometrical object such as a planar slab). The bismuth chalcogenides has been recently lined up with the category of artificial plasmonic materials. Such polar materials

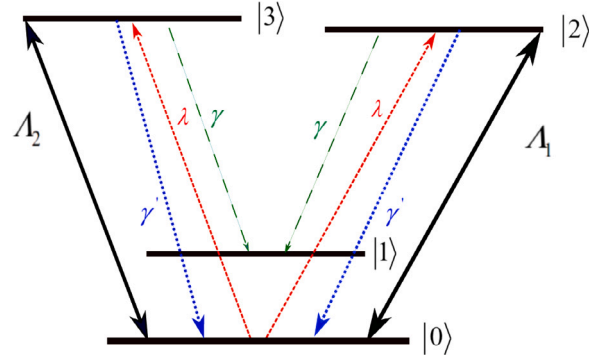


Fig. 1. Energy level diagram of the double-V type quantum emitter composed of two lower states $|0\rangle$ and $|1\rangle$ and two close-lying excited levels $|2\rangle$ and $|3\rangle$. The levels are coupled by a pair of weak spatially inhomogeneous probe beams A_1 and A_2 .

(Bi_2Se_3 and Bi_2Te_3) [57–61] support strong phonon resonances in the THz regime, which induce giant values in their dielectric function and hence sustain strong field concentration at their surfaces. The high-field values at the bismuth-chalcogenide surfaces lead to strong interaction between QEs and light [62]. We numerically study the consequences of spontaneous emission interference induced by the presence of bismuth-chalcogenide microstructures on the imposed torque for the double-V QEs. We show that the detection of this QI induced by the Bi_2Te_3 surface allows for a remote distance control of the light-induced torque and the resulting current flow.

We note that Au/Ag surfaces can also lead to the much desired enhancement of quantum interference due to surface-plasmon excitation [52], but this will happen in a very different frequency range than the THz regime which is used here (the enhancement happens in the visible regime of the spectrum) and also for significantly smaller distances (for few tens of nanometers from the surface of the metallic surface) and not for few micrometers from the surface that we present here. In addition, a comparison between the two schemes reveals that the enhancement of QI from a Bi_2Te_3 surface is more pronounced and for a much wider range of frequencies and distances of the QE from the surface [60,61] than from an Au or Ag surface.

2. Theory and method

2.1. The double-V-model light-matter interaction scheme

We begin with a simple model of a QE in double-V configuration which has two lower states $|0\rangle$ and $|1\rangle$ and a set of states $|2\rangle$ and $|3\rangle$ that can serve as two closely lying upper states. Generally, such a scheme can be realized in atoms, molecules, or quantum dots. The level diagram for such a model is shown in Fig. 1. The excited levels $|2\rangle$ and $|3\rangle$ decay to the lower states $|1\rangle$ and $|0\rangle$ with decay rates γ_{21}, γ_{31} ($\gamma_{21} = \gamma_{31} = \gamma$) and $\gamma'_{21}, \gamma'_{31}$ ($\gamma'_{21} = \gamma'_{31} = \gamma'$), respectively. Two incoherent pumping fields λ_1 and λ_2 ($\lambda_1 = \lambda_2 = \lambda$) pump populations from the lower state $|1\rangle$ to excited states $|2\rangle$ and $|3\rangle$, playing the role of a one-way pump process. A pair of weak spatially inhomogeneous counter-propagating probe fields A_1 and A_2 couple the lower states to the set of upper states.

The Hamiltonian describing the matter-light interaction can be written in the interaction representation as

$$H = \hbar \left(-\delta - \frac{\omega_{32}}{2} \right) |2\rangle\langle 2| + \hbar \left(-\delta + \frac{\omega_{32}}{2} \right) |3\rangle\langle 3| - (\hbar A_1 |0\rangle\langle 2| + \hbar A_2 |0\rangle\langle 3| + \text{H.c.}), \quad (1)$$

where $\delta = \omega - \bar{\omega}$ is the detuning from resonance with the average transition energies of upper states $|2\rangle$ and $|3\rangle$ from state $|0\rangle$ with $\bar{\omega} = (\omega_2 + \omega_3)/2 - \omega_0$. Note that $\omega_{32} = (\omega_3 - \omega_2)/2$ is the level splitting between

the excited sublevels and ω shows the angular frequency (we assume that both fields have equal frequencies ω). In addition, $\hbar\omega_i$ ($i = 0 - 3$) denotes the energy of state $|i\rangle$.

A double-V-model QE setup, such as the one proposed in our work, can be implemented experimentally in various atomic systems. For example, it can be realized using two $J = 0$ states for the lower states, $|0\rangle$ and $|1\rangle$, and $M = \pm 1$ sublevels of a $J = 1$ state for excited states $|2\rangle$ and $|3\rangle$. The energy difference $\hbar\omega_{32}$ between these excited states can be changed by applying a static magnetic field. In addition, the QE may be realized in hyperfine sublevels of the D lines in alkali-metal atoms, such as ^{85}Rb and ^{87}Rb [63–65]. Alternatively, the QE can also be implemented in dual CdSe/ZnS/CdSe quantum dots, where two quantum dots are coupled through a shared ZnS layer, enabling the formation of an effective double-V model [63]. These examples demonstrate the versatility of the double-V model and the potential for its experimental realization in various physical systems

2.2. Light-induced torque for the system

Let us assume that the two incident beams A_1 and A_2 are interacting with two legs of the lower V subsystem of the four-level double-V model QE illustrated in Fig. 1. Beams A_1 and A_2 are position-dependent functions representing the interaction in the electric dipole approximation expressed by $A_1 = \Omega_1 e^{i\theta_1(\mathbf{R})}$ and $A_2 = \Omega_2 e^{i\theta_2(\mathbf{R})}$ where $\theta_1(\mathbf{R}) = -l\phi + kz$, $\theta_2(\mathbf{R}) = -l\phi - kz$ are the phase functions associated with the light beams, and Ω_1 and Ω_2 are functions representing the Rabi frequencies, which for the doughnut Laguerre–Gaussian (LG) beams with the same spatial dependence take the form $\Omega_1 = |\Omega_1| \left(\frac{r}{w}\right)^{|l|} e^{-r^2/w^2}$ and $\Omega_2 = |\Omega_2| \left(\frac{r}{w}\right)^{|l|} e^{-r^2/w^2}$.

Here, r describes a cylindrical radius, l is an integer describing the topological (OAM) number, ϕ denotes the azimuthal angle, w is a beam waist, and $|\Omega_1|$ and $|\Omega_2|$ represent the strength of the position dependent beams. Note that we are interested in effects arising near the beam waist situated in the plane $z = 0$.

Assuming that the many-body wave function of the trapped emitters can be well approximated by the product of identical single-QE wave functions, each QE receives an identical force due to the light. The single body wave function can be separated into the product of internal and center-of-mass wave functions. The scattering force acting on the center-of-mass coordinate \mathbf{R} would then involve only the density matrix elements of the internal states:

$$\mathbf{F} = 2\hbar \left[\nabla\theta_1(\mathbf{R})\Omega_1(\rho_{20} + \rho_{02}) + \nabla\theta_2(\mathbf{R})\Omega_2(\rho_{30} + \rho_{03}) \right], \quad (2)$$

where the coherences ρ_{20} and ρ_{30} are density matrix elements for the probe transitions.

Using (2) and the spatial shape of the beams, one gets, for the force

$$\mathbf{F} = 2\hbar k\psi \left(\frac{r}{w}\right)^{2|l|} e^{-2r^2/w^2} \hat{z} + \frac{2\hbar l}{r} \tau \left(\frac{r}{w}\right)^{2|l|} e^{-2r^2/w^2} \hat{\phi}, \quad (3)$$

where

$$\psi = \Omega_2(\rho_{30} + \rho_{03}) - \Omega_1(\rho_{20} + \rho_{02}) = 2 \left[\Omega_2 \text{Re}(\rho_{30}) - \Omega_1 \text{Re}(\rho_{20}) \right], \quad (4)$$

$$\tau = -\Omega_1(\rho_{20} + \rho_{02}) - \Omega_2(\rho_{30} + \rho_{03}) = -2 \left[\Omega_1 \text{Re}(\rho_{20}) + \Omega_2 \text{Re}(\rho_{30}) \right]. \quad (5)$$

Note that in Eq. (3) carets denote unit vectors in cylindrical coordinates. To calculate the torque on the center of mass of the atoms about the beam axis, we need a component of the cross product of the position vector and force vector that is parallel to the beam axis. Since the position vector has components in the radial and vertical directions, and the force vector has components in the azimuthal and vertical directions, we only need to consider the cross product of the unit vectors in the radial and azimuthal directions, which gives a vector in the vertical direction. This is the only component that contributes to

the torque about the beam axis. The induced torque acting on the center of mass of the QEs about the beam axis then reads

$$\mathbf{T} = \mathbf{r} \times \mathbf{F} = 2\hbar l \left(\frac{r}{w}\right)^{2|l|} e^{-2r^2/w^2} \tau \hat{z}, \quad (6)$$

indicating a quantized induced torque rotating the QEs that increases for larger topological numbers. The torque has clearly the form of a doughnut with a maximum intensity region, establishing an optical dipole potential trap attracting the QEs. The torque is maximum in the toroidal region, and its magnitude changes with the controlling parameters of the system through the density matrix elements ρ_{20} and ρ_{30} entering the function τ , Eq. (5). This allows to control and even enhance the torque experienced by the QEs, thus generating an intensity-controllable ring-shaped flow. In what follows we evaluate the torque function τ by obtaining the analytical solutions to the density matrix elements ρ_{20} and ρ_{30} , and show how the system parameters can affect the variation of the induced torque.

2.3. Analytical solutions for the density matrix equations in the steady state

To elucidate the dynamics of the populations and coherences, we can proceed using the Liouville equation of motion for the density matrix, using Eq. (1), and then use the Weisskopf–Wigner theory of spontaneous emission [66] to obtain the following equations [40,41,67]:

$$\dot{\rho}_{20} = (i\delta + \frac{i\omega_{32}}{2} - \gamma - \gamma' - \lambda)\rho_{20} + i\Omega_1(\rho_{00} - \rho_{22}) - i\Omega_2\rho_{23} - \kappa\rho_{30}, \quad (7)$$

$$\dot{\rho}_{30} = (i\delta - \frac{i\omega_{32}}{2} - \gamma - \gamma' - \lambda)\rho_{30} + i\Omega_2(\rho_{00} - \rho_{33}) - i\Omega_1\rho_{32} - \kappa\rho_{20}, \quad (8)$$

$$\dot{\rho}_{23} = (i\omega_{32} - 2\gamma - 2\gamma')\rho_{23} + i\Omega_1\rho_{03} - i\Omega_2\rho_{20} - \kappa(\rho_{22} + \rho_{33}), \quad (9)$$

$$\dot{\rho}_{22} = -2(\gamma + \gamma')\rho_{22} + \lambda\rho_{00} + i\Omega_1(\rho_{02} - \rho_{20}) - \kappa(\rho_{23} + \rho_{32}), \quad (10)$$

$$\dot{\rho}_{33} = -2(\gamma + \gamma')\rho_{33} + \lambda\rho_{00} + i\Omega_2(\rho_{03} - \rho_{30}) - \kappa(\rho_{23} + \rho_{32}), \quad (11)$$

$$\dot{\rho}_{00} = 2\gamma'(\rho_{22} + \rho_{33}) - 2\lambda\rho_{00} - i\Omega_1(\rho_{02} - \rho_{20}) - i\Omega_2(\rho_{03} - \rho_{30}), \quad (12)$$

constrained by $\rho_{11} + \rho_{22} + \rho_{33} = 1$ and $\rho_{ij} = \rho_{ji}^*$.

The term κ in the above equations is defined by $\kappa = p\sqrt{\gamma_{21}\gamma_{31}}$, which for $\gamma_{21} = \gamma_{31} = \gamma$ reduces to $\kappa = p\gamma$. This term is the result of QI of spontaneous emission from the two close-lying upper levels $|2\rangle$ and $|3\rangle$. The parameter p describes the degree of QI and denotes the alignment of the two matrix elements. It is defined by $p = \bar{\mu}_{21} \cdot \bar{\mu}_{31} / |\bar{\mu}_{21}| |\bar{\mu}_{31}| = \cos\theta$, where $\bar{\mu}_{21}$ and $\bar{\mu}_{31}$ are the transition dipole moments. Such a QI plays a crucial role in creating the coherence [40,41]. Obviously, the QI term κ depends strongly on the orientations of the dipole polarizations. If they are close to parallel, then $\kappa \rightarrow \gamma$ ($p \rightarrow 1$) and the interference effect is close to maximal; while if they are perpendicular, then $\kappa = 0$ and the QI disappears.

Under the steady-state condition, from Eqs. (7)–(12), the solutions for the off-diagonal density matrix ρ_{20} and ρ_{30} read Eqs. (13) and (14) are given in Box I, where $\rho_{23} = \rho_{32}^* = \frac{\kappa(\rho_{22} + \rho_{33})}{i\omega_{32} - 2(\gamma + \gamma')}$. The numerators in Eqs. (13) and (14) consist of two parts. The first two terms in each numerator stem from the direct transitions $|1\rangle \rightarrow |2\rangle$, $|1\rangle \rightarrow |3\rangle$ and depend on the population inversions ($\rho_{ii} - \rho_{00}$) ($i = 2, 3$). The next two terms are due to the emergence of the QI which is proportional to the coherence terms ρ_{32} and ρ_{23} .

We are also interested in this paper on the absorption properties of the system. The absorption/gain in the medium corresponds to the imaginary part of the electric susceptibility

$$\chi(\delta) = \frac{2N|\bar{\mu}|^2}{\epsilon_0\hbar} \left(\frac{\rho_{20}}{\Omega_1} + \frac{\rho_{30}}{\Omega_2} \right), \quad (15)$$

where we have assumed $|\bar{\mu}_{21}| = |\bar{\mu}_{31}| = |\bar{\mu}|$. Here, ϵ_0 is the vacuum permittivity and N is the density of the QEs. In the limit of weak light-matter interaction, one can find, to the zero-order of Ω_1 and Ω_2 :

$$\rho_{22} = \rho_{33} = \frac{2\lambda(\gamma + \gamma') \left[4(\gamma + \gamma')^2 + \omega_{32}^2 \right]}{-16\kappa^2(\gamma + \gamma')^2 + 4 \left[4(\gamma + \gamma')^2 + \omega_{32}^2 \right] \left[(\gamma + \gamma')^2 + \lambda(\gamma + \gamma') \right]}, \quad (16)$$

$$\rho_{20} = \frac{i\Omega_2\kappa(\rho_{33} - \rho_{00}) + i\Omega_1(i\delta - \frac{i\omega_{32}}{2} - \gamma - \gamma' - \lambda)(\rho_{22} - \rho_{00}) + i\Omega_1\kappa\rho_{32} + i\Omega_2(i\delta - \frac{i\omega_{32}}{2} - \gamma - \gamma' - \lambda)\rho_{23}}{(i\delta + \frac{i\omega_{32}}{2} - \gamma - \gamma' - \lambda)(i\delta - \frac{i\omega_{32}}{2} - \gamma - \gamma' - \lambda) - \kappa^2}, \quad (13)$$

$$\rho_{30} = \frac{i\Omega_1\kappa(\rho_{22} - \rho_{00}) + i\Omega_2(\delta + \frac{i\omega_{32}}{2} - \gamma - \gamma' - \lambda)(\rho_{33} - \rho_{00}) + i\Omega_2\kappa\rho_{23} + i\Omega_1(\delta + \frac{i\omega_{32}}{2} - \gamma - \gamma' - \lambda)\rho_{32}}{(i\delta + \frac{i\omega_{32}}{2} - \gamma - \gamma' - \lambda)(i\delta - \frac{i\omega_{32}}{2} - \gamma - \gamma' - \lambda) - \kappa^2}, \quad (14)$$

Box I.

$$\rho_{00} = \frac{-16\kappa^2(\gamma + \gamma')^2 + 4(\gamma + \gamma')^2 [4(\gamma + \gamma')^2 + \omega_{32}^2]}{-16\kappa^2(\gamma + \gamma')^2 + 4 [4(\gamma + \gamma')^2 + \omega_{32}^2] [(\gamma + \gamma')^2 + \lambda(\gamma + \gamma')]}, \quad (17)$$

$$\rho_{23} = \frac{-4\lambda\kappa(\gamma + \gamma')(i\omega_{32} + 2\gamma + 2\gamma')}{-16\kappa^2(\gamma + \gamma')^2 + 4 [4(\gamma + \gamma')^2 + \omega_{32}^2] [(\gamma + \gamma')^2 + \lambda(\gamma + \gamma')]} \quad (18)$$

$$\rho_{11} = 1 - \rho_{00} - \rho_{22} - \rho_{33}. \quad (19)$$

3. Results

Eqs. (6) and (15) together with Eqs. (13), (14) and (16)–(19) show that the variation of torque and electric susceptibility with changing probe detuning δ depends on the system parameters, i.e., the rate of incoherent pump r , the doublet splitting ω_{32} , the QI parameter κ , the strengths of laser fields $|\Omega_1|$, $|\Omega_2|$, and the free-space spontaneous decay rate γ' . With or without the free-space spontaneous decay rate, both torque and electric susceptibility are seen to be surprisingly dependent on the particular initial states of the QE. Next, we will consider the following situations: (1) QE initially in an antisymmetric state; (2) QE initially in a symmetric state. We also investigate the effect of a bismuth-chalcogenide photonic microstructure on the induced torque on QEs.

3.1. Case 1: QE initially in an antisymmetric state

Let us first assume a situation where the upper levels $|2\rangle$ and $|3\rangle$ are degenerate ($\omega_{32} = 0$), the incoherent pump λ is present in the system ($\lambda \neq 0$) and free-space spontaneous decay rate is zero ($\gamma' = 0$). We also consider the case of perfect interference $\kappa = \gamma$ ($p = 1$). In such a situation one gets easily from Eqs. (16)–(18) the density matrix elements

$$\rho_{00} = 0, \quad \rho_{22} = \rho_{33} = \frac{1}{2}, \quad \rho_{23} = -\frac{1}{2}, \quad (20)$$

indicating that the QE is initially in an antisymmetric state $|D\rangle = \frac{|2\rangle - |3\rangle}{\sqrt{2}}$. Substituting Eq. (20) into Eqs. (13) and (14) yields

$$\rho_{20} = \frac{i(\Omega_1 - \Omega_2)}{2(i\delta - \lambda)}, \quad (21)$$

$$\rho_{30} = \frac{i(\Omega_2 - \Omega_1)}{2(i\delta - \lambda)}. \quad (22)$$

Clearly, when $\Omega_1 = \Omega_2$, then $\rho_{20} = \rho_{30} = 0$. This is the case of optical transparency for all frequencies of the probe fields $\text{Im}(\chi) = 0$. Illustrating this feature is the dashed line in Fig. 2(a) for $|\Omega_1| = |\Omega_2| = 0.1\gamma$. Such a transparency is due to the population trapping, and is attributed to the population inversion without lasing [39]. The torque is subsequently zero for all frequency detunings, as can be seen from the dashed line in Fig. 3(b). Note that the torque function given in Eq. (5) depends on the position dependent Rabi-frequencies Ω_1 and Ω_2 (LG beams). However, as we consider that the QEs are trapped in the ring of a LG beam, then the Rabi frequencies are almost constant there, meaning that the plots for $|\Omega_1|$ and $|\Omega_2|$ are valid to a very good approximation.

The torque can be made non-zero when $\Omega_1 \neq \Omega_2$ for the all frequencies of probe detuning except $\delta = 0$, as can be seen from solid line in Fig. 2(b). One can find that the torque has a dispersive behavior with a negative slope, vanishing at $\delta = 0$. Eq. (5) attributes

the induced torque to the real part of optical coherences ρ_{21} and ρ_{31} . However, Eqs. (21) and (22) demonstrate that these coherences are purely imaginary for the resonance of the probe fields ($\rho_{20}(\delta = 0) = -\rho_{30}(\delta = 0) = \frac{i(\Omega_2 - \Omega_1)}{\lambda}$), suppressing the induced torque at $\delta = 0$. Such a torque experiences an absorption for $\Omega_1 \neq \Omega_2$ (see the solid line in Fig. 2(a)) given by

$$\text{Im}[\chi(\delta)] = \frac{2N|\bar{\mu}|^2}{\epsilon_0\hbar} \left(\frac{\lambda(\frac{\Omega_1 - \Omega_2}{\Omega_1\Omega_2})^2}{2\lambda^2 + 2\delta^2} \right). \quad (23)$$

We repeat the same calculations as above, but for the case of no QI, i.e., $\kappa = 0$ ($p = 0$). In this case, Eqs. (16)–(18) reduce to

$$\rho_{00} = \frac{16\gamma^4}{16\gamma^4 + 16r\gamma^3} = \frac{\gamma^4}{\gamma^4 + \lambda\gamma^3}, \quad (24)$$

$$\rho_{22} = \rho_{33} = \frac{8\lambda\gamma^3}{16\gamma^4 + 16\lambda\gamma^3} = \frac{1}{2} \frac{\lambda\gamma^3}{\gamma^4 + \lambda\gamma^3}, \quad \rho_{23} = 0,$$

which for $\lambda = \gamma$ simplifies more to

$$\rho_{00} = \frac{1}{2}, \quad \rho_{22} = \rho_{33} = \frac{1}{4}, \quad \rho_{23} = 0. \quad (25)$$

Obviously, the system no longer remains in antisymmetric state $|D\rangle = \frac{|2\rangle - |3\rangle}{\sqrt{2}}$ when the QI is not taken into account (i.e., $p = \kappa = 0$).

Calling on Eq. (25), Eqs. (13) and (14) can be rewritten as

$$\rho_{20} = \frac{-i\Omega_1}{4(i\delta - 2\gamma)}, \quad (26)$$

$$\rho_{30} = \frac{-i\Omega_2}{4(i\delta - 2\gamma)}. \quad (27)$$

Illustrated in Fig. 3(b), the nonresonant torque is always nonzero either for $\Omega_1 = \Omega_2$ (dashed line) or $\Omega_1 \neq \Omega_2$ (solid line), accompanied by the probe absorption

$$\text{Im}[\chi(\delta)] = \frac{2N|\bar{\mu}|^2}{\epsilon_0\hbar} \left(\frac{\gamma}{4\gamma^2 + \delta^2} \right). \quad (28)$$

The magnitude of torque is rather small in this case, similar to Fig. 2(b), with the only difference being the fact that the slope of the torque function is now converted to positive (see Fig. 3(b)).

Note that if $\gamma' \neq 0$ (with the free-space spontaneous decay rate), Eqs. (16)–(18) change to

$$\rho_{22} = \rho_{33} = \frac{8\lambda(\gamma + \gamma')^3}{16(\gamma + \gamma')^2 [(\gamma + \gamma')^2 - \kappa^2] + 16\lambda(\gamma + \gamma')^3}, \quad (29)$$

$$\rho_{00} = \frac{16(\gamma + \gamma')^2 [(\gamma + \gamma')^2 - \kappa^2]}{16(\gamma + \gamma')^2 [(\gamma + \gamma')^2 - \kappa^2] + 16\lambda(\gamma + \gamma')^3}, \quad (30)$$

$$\rho_{23} = \frac{-8\lambda\kappa(\gamma + \gamma')^2}{16(\gamma + \gamma')^2 [(\gamma + \gamma')^2 - \kappa^2] + 16\lambda(\gamma + \gamma')^3}, \quad (31)$$

indicating that the presence of the free-space spontaneous decay rate γ' destroys the dark state $|D\rangle = \frac{|2\rangle - |3\rangle}{\sqrt{2}}$, even if the QI is present.

3.2. Case 2: QE initially in a symmetric state

Next we consider a situation that $\omega_{32} \neq 0$ (nondegenerate upper levels) but $\lambda = 0$ (the incoherent pump r is absent in the system). In

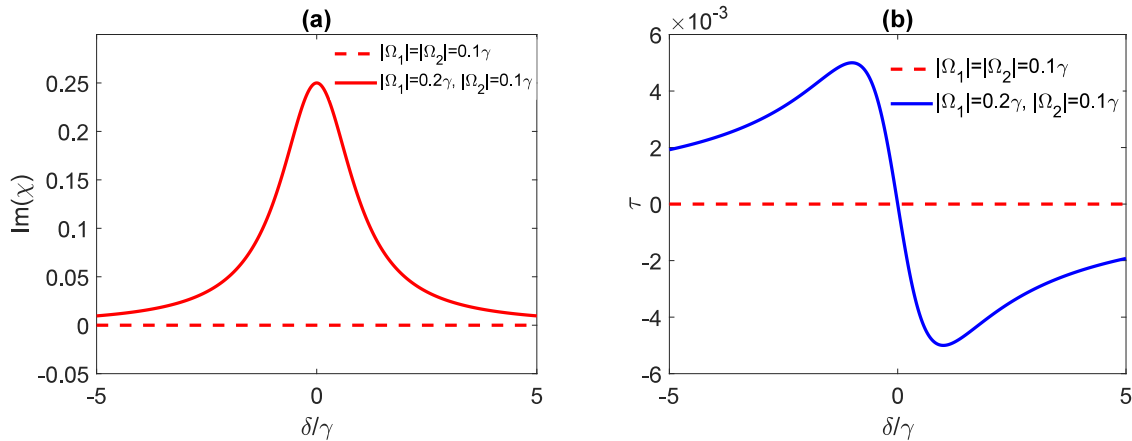


Fig. 2. (a) The absorption (gain) spectrum $\text{Im}(\chi)$ (in units of $\frac{2N|\bar{\mu}|^2}{\epsilon_0\hbar}$) and (b) the induced torque function τ (in units of s^{-1}) as a function of detuning δ (in units of γ). (b) Here, $\gamma' = 0$, $\omega_{32} = 0$, $\lambda = \gamma$, $p = 1$ (or $\kappa = \gamma$), and for different strengths $|\Omega_1| = |\Omega_2| = 0.1\gamma$ (dashed line) and $|\Omega_1| = 0.2\gamma$, $|\Omega_2| = 0.1\gamma$ (solid line).

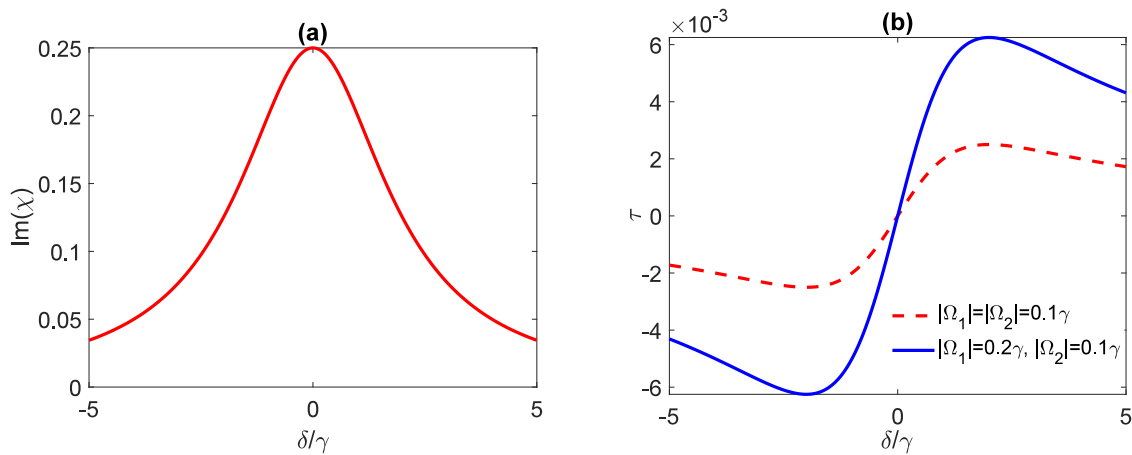


Fig. 3. (a) The absorption (gain) spectrum $\text{Im}(\chi)$ (in units of $\frac{2N|\bar{\mu}|^2}{\epsilon_0\hbar}$) and (b) the induced torque function τ (in units of s^{-1}) as a function of detuning δ (in units of γ). (b) Here, $\gamma' = 0$, $\omega_{32} = 0$, $\lambda = \gamma$, $p = 0$ (or $\kappa = 0$), and for different strengths $|\Omega_1| = |\Omega_2| = 0.1\gamma$ (dashed line) and $|\Omega_1| = 0.2\gamma$, $|\Omega_2| = 0.1\gamma$ (solid line).

this case, Eqs. (16)–(18) reduce to

$$\rho_{00} = 1, \quad \rho_{22} = \rho_{33} = 0, \quad \rho_{23} = 0, \quad (32)$$

representing a situation where the QE is in the ground state $|0\rangle$ (or in the symmetric state $|B\rangle = \frac{|2\rangle+|3\rangle}{\sqrt{2}}$). Note that Eq. (32) is valid for any values of p (perfect $p = 1$ or imperfect $p \neq 1$ quantum interference). Using Eq. (32) as the particular initial state of the QE, Eqs. (13) and (14) change to

$$\rho_{20} = -i \frac{\Omega_2\kappa + \Omega_1(i\delta - \frac{i\omega_{32}}{2} - \gamma)}{(i\delta + \frac{i\omega_{32}}{2} - \gamma)(i\delta - \frac{i\omega_{32}}{2} - \gamma) - \kappa^2}, \quad (33)$$

$$\rho_{30} = -i \frac{\Omega_1\kappa + \Omega_2(i\delta + \frac{i\omega_{32}}{2} - \gamma)}{(i\delta + \frac{i\omega_{32}}{2} - \gamma)(i\delta - \frac{i\omega_{32}}{2} - \gamma) - \kappa^2}. \quad (34)$$

The probe absorption in this case becomes

$$\text{Im}[\chi(\delta)] = \frac{2N|\bar{\mu}|^2}{\epsilon_0\hbar} \left(\frac{as + 4\delta^2\gamma}{4\gamma^2\delta^2 + a^2} \right), \quad (35)$$

where $a = -\kappa^2 + \gamma^2 - \delta^2 + \frac{\omega_{32}^2}{4}$ and $s = 2\gamma - \kappa \frac{\Omega_1^2 + \Omega_2^2}{\Omega_1\Omega_2}$. For the perfect QI situation $\kappa = \gamma$ ($p = 1$), and for $\Omega_1 = \Omega_2$ and $\delta = 0$, one gets $s = 0$, yielding $\text{Im}[\chi(0)] = 0$ (optical transparency). For $\Omega_1 \neq \Omega_2$ (in our case $\Omega_1 = 2\Omega_2$), $s < 0$, resulting in $\text{Im}[\chi(0)] < 0$ (optical gain). In the absence of quantum interference, $p = \kappa = 0$, the same initial condition as Eq. (32) holds. Setting $\kappa = 0$ in Eqs. (33) and (34), one

has

$$\rho_{21} = -i \frac{\Omega_1}{(i\delta + \frac{i\omega_{32}}{2} - \gamma)}, \quad (36)$$

$$\rho_{31} = -i \frac{\Omega_2}{(i\delta - \frac{i\omega_{32}}{2} - \gamma)}, \quad (37)$$

leading to

$$\text{Im}[\chi(\delta)] = \frac{2N|\bar{\mu}|^2}{\epsilon_0\hbar} \left(\frac{2\gamma(\gamma^2 - \delta^2 + \frac{\omega_{32}^2}{4}) + 4\delta^2\gamma}{4\gamma^2\delta^2 + (\gamma^2 - \delta^2 + \frac{\omega_{32}^2}{4})^2} \right). \quad (38)$$

Numerical simulations for the absorption/gain spectrum of case 2 for $p = 1$ ($p = 0$) are illustrated in Fig. 4(a) (Fig. 5(a)) for $\Omega_1 = \Omega_2$ and $\Omega_1 \neq \Omega_2$. Clearly, if QI is taken into account and for $|\Omega_1| = |\Omega_2| = 0.1\gamma$, the transparency window appears around the line center (the dashed line in Fig. 4(a)). On the other hand, the medium starts to experience gain on resonance (the solid line in Fig. 4(a)) if $\Omega_1 \neq \Omega_2$. This is an example of lasing without population inversion (see also Eq. (32)) which is achieved in the presence of QI. The medium becomes absorptive again if the interference is neglected ($p = 0$), as seen in Fig. 5(a) and Eq. (38). We present in Figs. 4(b) and 5(b) how the induced torque behaves in the particular case 2. In the presence of QI and for $|\Omega_1| = |\Omega_2| = 0.1\gamma$ (the dashed line in Fig. 4(b), with the inset with a zoomed-in feature), the profile shows a dispersive behavior with a negative slope around the zero detuning and a magnitude comparable with those observed in

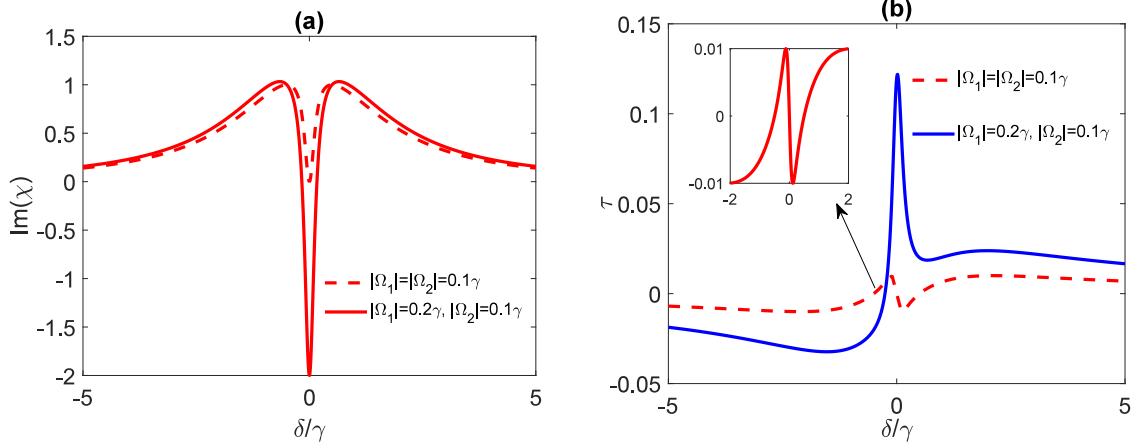


Fig. 4. (a) The absorption (gain) spectrum $\text{Im}(\chi)$ (in units of $\frac{2N|\vec{\mu}|^2}{\epsilon_0\hbar}$) and (b) the induced torque function τ (in units of s^{-1}) as a function of detuning δ (in units of γ). (b) Here, $\gamma' = 0$, $\omega_{32} = \gamma$, $\lambda = 0$, $p = 1$ (or $\kappa = \gamma$), and for different strengths $|\Omega_1| = |\Omega_2| = 0.1\gamma$ (dashed line) and $|\Omega_1| = 0.2\gamma$, $|\Omega_2| = 0.1\gamma$ (solid line).

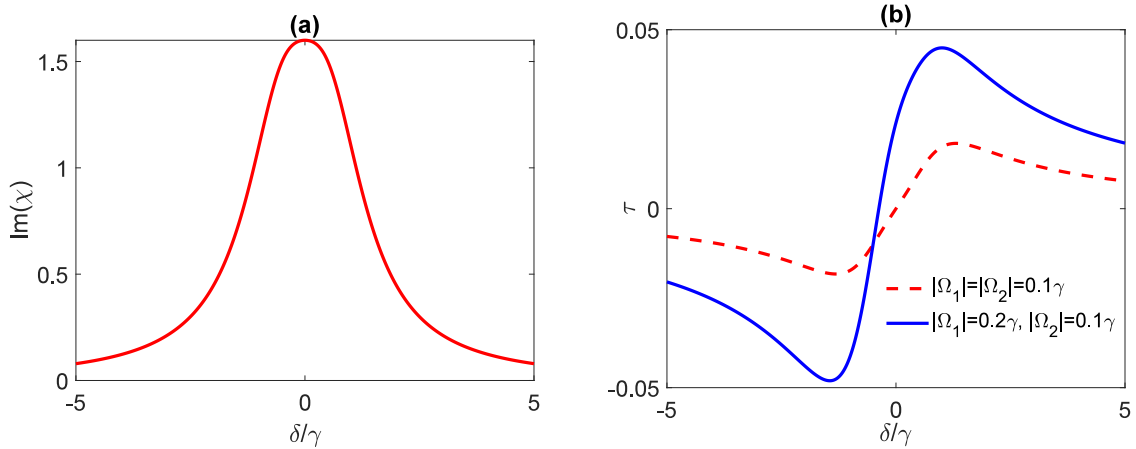


Fig. 5. (a) The absorption (gain) spectrum $\text{Im}(\chi)$ (in units of $\frac{2N|\vec{\mu}|^2}{\epsilon_0\hbar}$) and (b) the induced torque function τ (in units of s^{-1}) as a function of detuning δ (in units of γ). (b) Here, $\gamma' = 0$, $\omega_{32} = \gamma$, $\lambda = 0$, $p = 0$ (or $\kappa = 0$), and for different strengths $|\Omega_1| = |\Omega_2| = 0.1\gamma$ (dashed line) and $|\Omega_1| = 0.2\gamma$, $|\Omega_2| = 0.1\gamma$ (solid line).

case 1 (Figs. 2(b) and 3(b)), which vanishes at $\delta = 0$. The torque can be made non-zero even on resonance $\delta = 0$ for $|\Omega_1| = 0.2\gamma$, $|\Omega_2| = 0.1\gamma$ (solid line in Fig. 4(b)). In this case, the torque shows a resonant-like behavior and reaches a maximum which is larger compared to previous cases. The magnitude torque can be further enhanced for other values of $|\Omega_1|$ and $|\Omega_2|$, e.g., $|\Omega_1| = 0.3\gamma$, $|\Omega_2| = 0.1\gamma$ (not shown in the paper). If the dipole moments are perpendicular (no QI i.e., $\kappa = 0$) (Fig. 5(b)), the profiles of the induced torque are very similar to Fig. 3. Therefore, the presence of QI, along with proper preparation of the initial state of the QE allows the emergence of a resonant non-zero enhanced torque.

Considering Eq. (32) as the initial state of the QE, one can investigate the effect of γ' on the variation of induced torque. The numerical results for the case of nonzero free-space spontaneous decay rate are rather similar qualitatively for both the absorption and torque as for the case of zero free-space decay $\gamma' = 0$ (not shown here). However, no transparency is achieved for nonzero decay rate γ' when $|\Omega_1| = |\Omega_2|$. Moreover, the minimum of the gain dip is less when $|\Omega_1| \neq |\Omega_2|$. In the presence of γ' , Eq. (35) takes a more complex form as

$$\text{Im}[\chi(\delta)] = \frac{2N|\vec{\mu}|^2}{\epsilon_0\hbar} \left(\frac{a's' + 4\delta^2\gamma}{4\gamma^2\delta^2 + a'^2} \right), \quad (39)$$

with $a' = -\kappa^2 + (\gamma + \gamma')^2 - \delta^2 + \frac{\omega_{32}^2}{4}$ and $s' = 2(\gamma + \gamma') - \kappa \frac{\Omega_1^2 + \Omega_2^2}{\Omega_1\Omega_2}$. Obviously, when $|\Omega_1| = |\Omega_2|$ and for the perfect QI case $\kappa = \gamma$, $\text{Im}[\chi(\delta = 0)] > 0$ ($\text{Im}[\chi(\delta = 0)] / \frac{2N|\vec{\mu}|^2}{\epsilon_0\hbar} = 2\gamma'$) demonstrating a small

absorption on resonance. On the other hand, when $|\Omega_1| \neq |\Omega_2|$, one gets $s < s' < 0$, leading to a less deep amplification.

3.3. Effect of bismuth-chalcogenide microstructures

The QI effect is generated when two closely lying upper levels of the double-V-model QE ($|2\rangle$ and $|3\rangle$) decay to the common level $|1\rangle$ so that the corresponding spontaneous-emission channels can interfere. We have investigated the influence of this interference on the light-induced torque in the previous subsections. The essence of such interference effect requires a very meticulous condition to be valid, viz., the dipole matrix moments for two close-lying states $|2\rangle$ and $|3\rangle$ spontaneously decaying to the common state $|1\rangle$ should be nonorthogonal, otherwise, the quantum interference does not exist. This can be a problem for usual quantum systems (atoms, molecules, and quantum dots) as they mostly allow the orthogonal dipole matrix elements, preventing the QI from occurring. Nevertheless, an anisotropic quantum vacuum has been predicted to induce QI during the spontaneous emission process when placing the QEs in the neighborhood of a photonic structure, as predicted by Agarwal [50].

Taking advantage of this idea, in what follows we examine how light induces a torque on the double-V QEs when they are placed in the vicinity of a bismuth-chalcogenide Bi_2Te_3 microstructure. Fig. 6 demonstrates the setup where the double-V QE is located at distance d above the planar surface of the topological insulator Bi_2Te_3 . We assume that the dipole moment of the QE interacting with the photonic

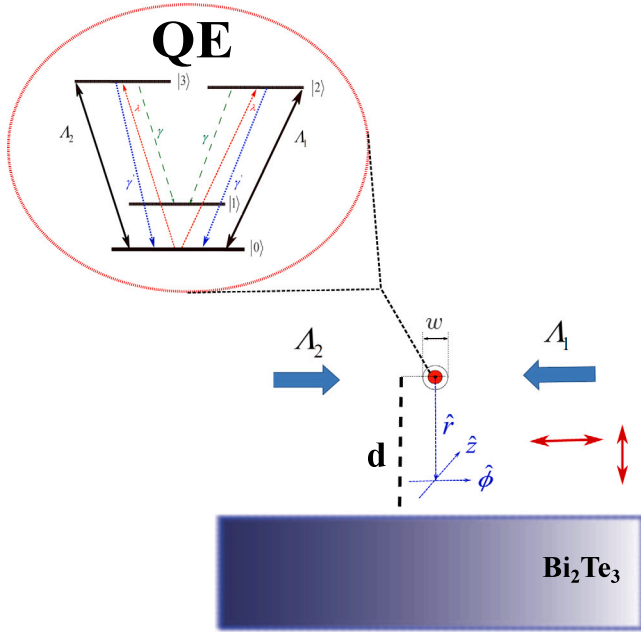


Fig. 6. QE in a photonic environment. The double-V QE lies at a distance d above the surface of a thick slab of Bi_2Te_3 , and is subject to two counterpropagating LG beams propagating along the $\hat{\phi}$ -direction, i.e., i.e. parallel to the surface of Bi_2Te_3 slab. The red arrows denote the two different oscillation orientations of the QE dipole moment. Air is taken to be the surrounding medium.

reservoir of modes of Bi_2Te_3 is oriented either horizontally or vertically, i.e. parallel or normal to the topological insulator Bi_2Te_3 surface.

Due to the presence of the photonic structure (bismuth-chalcogenide Bi_2Te_3), according to [61,68–70] and based on Appendix, the parameters γ and κ in previous section change to

$$\gamma = \frac{1}{2}(\Gamma_{\perp} + \Gamma_{\parallel}), \quad (40)$$

$$\kappa = \frac{1}{2}(\Gamma_{\perp} - \Gamma_{\parallel}), \quad (41)$$

where the values of the parameters Γ_{\perp} (normal) and Γ_{\parallel} (parallel) depend on the distance d between the QE and the planar surface of the Bi_2Te_3 slab [61]. It should be pointed out that, as depicted in Fig. 6, the motion of QE is restricted on a plane parallel to the material surface. This means that the values of Γ_{\perp} and Γ_{\parallel} will be the same for every QE position on the plane since the QEs remain constantly on the same plane. Another important point taken out of this geometry is the fact that one does not need to worry about the scattering of the LG beams from the material surface as the beams are assumed to propagate along the $\hat{\phi}$ -direction, i.e. parallel to the surface of Bi_2Te_3 insulator.

The term κ in Eq. (41) represents the coupling coefficient between states $|2\rangle$ and $|3\rangle$ (due to the spontaneous emission in a modified anisotropic vacuum [50]). The corresponding degree of quantum interference is defined then as $p = (\Gamma_{\perp} - \Gamma_{\parallel})/(\Gamma_{\perp} + \Gamma_{\parallel})$. Clearly, the QI plays a role when the QE is placed next to the Bi_2Te_3 surface. The value $|p| = 1$ corresponds to the maximum degree of quantum interference in the spontaneous emission [71]. This usually occurs when the emitter is placed in a proximity to the structure that can completely quench Γ_{\perp} . On the other hand, when the emitter lies in the free-space vacuum, one has $\Gamma_{\perp} = \Gamma_{\parallel} = \Gamma_0$ giving $\gamma = \Gamma_0$, $\kappa = 0$ and thus $p = 0$, so the QI is completely absent in the double-V-type QE. We have defined here Γ_0 as the decay rate in the vacuum to make it distinguishable from the decay rate γ in Eq. (40), influenced by the interaction with insulator surface.

The results of Γ_{\perp} (normal) and Γ_{\parallel} (parallel) as well as the degree of QI p as a function of the distance from the topological insulator Bi_2Te_3 are presented in Fig. 7(a,b) for two frequencies 2 THz and 4 THz, respectively.

We observe in Fig. 7(a) (Fig. 7(b)) that as the distance between the QE and the Bi_2Te_3 increases, the value of Γ_{\parallel} exhibits an initial strong decrease up to a distance approximately $d \approx 6 \mu\text{m}$ ($d \approx 3 \mu\text{m}$) for 2 THz (4 THz) while becoming significantly smaller than the free-space decay rate. As the distance increases further, its value raises weakly getting slightly larger than the free-space decay rate. In addition, the Γ_{\perp} value decreases for both frequencies with the increase of the distance between the QE and the bismuth-chalcogenide microstructure. Since Γ_{\perp} is much larger than Γ_{\parallel} in the region of $d \approx 6 \mu\text{m}$ ($d \approx 3 \mu\text{m}$) for 2 THz (4 THz), the corresponding QI factor p becomes maximum there (about 0.88–0.89 for 2 THz and slightly less for 4 THz).

To model the torque behaviors of the double-V QE next to the topological insulator we consider the case that $\omega_{32} \neq 0$ and $r = 0$ (similar to case (2) in the previous section). Note that the case (1) discussed in the previous section only exists when we get exactly maximum interference $p = 1$ ($\kappa = \gamma$), which cannot happen next to the Bi_2Te_3 . Figs. 8 and 9 show the variation of induced torque function τ with changing the distance of QE to the bismuth-chalcogenide microstructure for different frequencies in the THz regime, i.e., 2 THz and 4 THz, respectively. Illustrated in Fig. 8(a) (Fig. 9(a)), the QE experiences a very weak torque for the surface-emitter separations up to $d = 2.10 \mu\text{m}$ ($d = 0.66 \mu\text{m}$) for the frequency 2 THz (4 THz). When the distance d between the QE and Bi_2Te_3 surface increases gradually, the magnitude of induced torque increases and reaches a maximum value for $d = 6.10 \mu\text{m}$ ($d = 3 \mu\text{m}$) for which the degree of QI was the largest. The torque function τ start to reduce for larger distances, as can be seen in Fig. 8 (b) (Fig. 9(b)). We observe that the maximum torque achieved for the frequency 2 THz is larger in comparison with the one for the case of 4 THz. This is because the degree of QI for the frequency 2 THz is larger than the one for 4 THz (Fig. 7). Clearly, the maximum torque is now less than the one observed in solid line of Fig. 4(b) where the torque function τ was plotted for the same set of parameters but for the perfect QI situation $p = 1$ (the case that the QI was due to the nonorthogonality of dipole matrix elements for the two transitions). However, as the QI term κ depends now on the separation between the quantum emitter and the Bi_2Te_3 surface, it paves the way towards the remote distance control of the induced torque and the resulting current flow, the feature which was missing when the existence of QI was due to the nonorthogonality of dipole matrix elements.

Finally in Fig. 10 we present the variation of torque function against the doublet splitting ω_{32} for a separation distance $d = 3 \mu\text{m}$ and for the frequency 4 THz. We find that τ exhibits significant increase up to the splitting value $\omega_{32} \approx 1.5\Gamma_0$, and then starts to decrease, meaning that the magnitude of torque can be further enhanced via manipulating the doublet splitting ω_{32} .

4. Concluding remarks

In summary, we have investigated the effects of quantum interference in spontaneous emission on the light-induced torque in a four-level double-V type light-matter interaction scheme. When the double-V quantum emitters interact with a pair of spatially inhomogeneous weak laser fields, a quantized torque can be induced on the center of mass of each trapped QE. Such a torque is directly proportional to the topological charge of the inhomogeneous probe beams, rotates the whole ensemble about the beam axis, and creates a ring-shaped current flow. We analytically and numerically demonstrated how the quantum interference between the two excitation pathways in the upper V subsystem of the double-V QE with a closely spaced doublet can impose a controllable torque on the whole system. The magnitude of such an induced torque can be controlled by the initial internal state preparation of the QEs, and can be enhanced by the strength of the inhomogeneous beams. The system can experience absorption, transparency or lasing, depending on how the QE is initially populated.

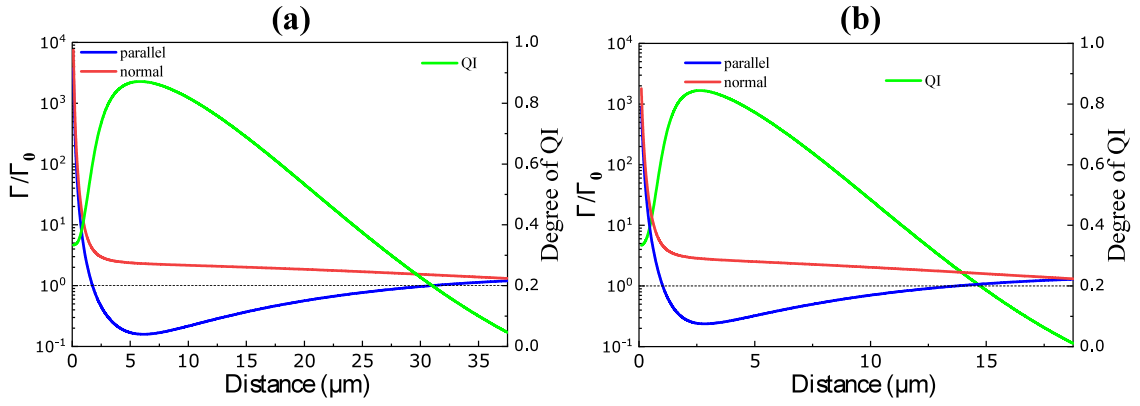


Fig. 7. The spontaneous decay rate for a dipole which is normally (\perp , red curve) and parallelly (\parallel , blue curve) oriented with respect to a plane of Bi_2Te_3 as well as the degree of QI, ρ (green curve), as a function of the distance from the planar surface of Bi_2Te_3 , for two frequencies 2 THz (a) and 4 THz (b). Note that Γ_0 is the decay rate in the vacuum.

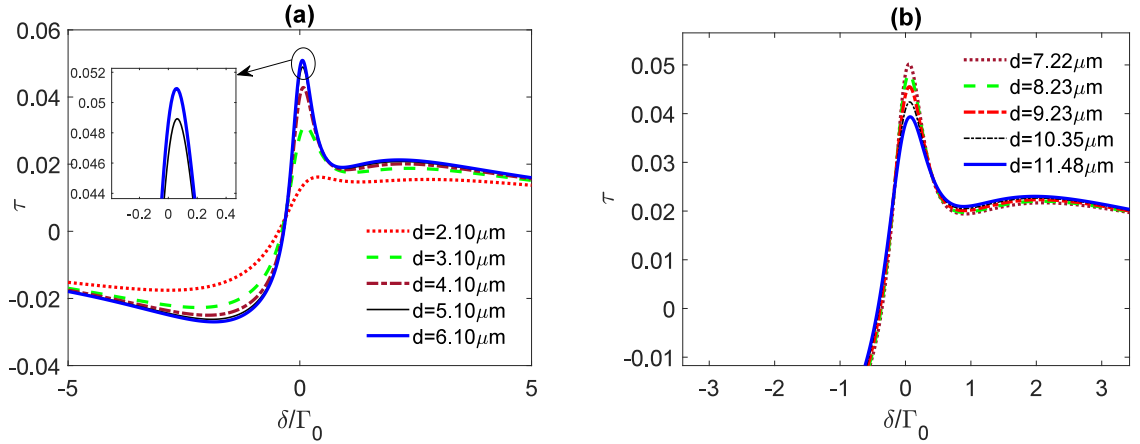


Fig. 8. (a) The variation of induced torque function τ (in units of s^{-1}) as a function of detuning δ (in units of γ) at the frequency 2 THz. Here, $\gamma' = 0$, $\omega_{32} = \Gamma_0$, $\lambda = 0$, $|\Omega_1| = 0.2\Gamma_0$, $|\Omega_2| = 0.1\Gamma_0$. (a) Shows the torque variation for distances $d = 2.10 \mu\text{m}$ (dotted line), $d = 3.10 \mu\text{m}$ (green dashed line), $d = 4.10 \mu\text{m}$ (dash-dotted line), $d = 5.10 \mu\text{m}$ (black dashed line), and $d = 6.10 \mu\text{m}$ (solid line), while (b) shows its variation for distances $d = 7.22 \mu\text{m}$ (dotted line), $d = 8.23 \mu\text{m}$ (dashed line), $d = 9.23 \mu\text{m}$ (red dash-dotted line), $d = 10.35 \mu\text{m}$ (black dash-dotted line) and $d = 11.48 \mu\text{m}$ (solid line). Note that Γ_0 is the decay rate in the vacuum.

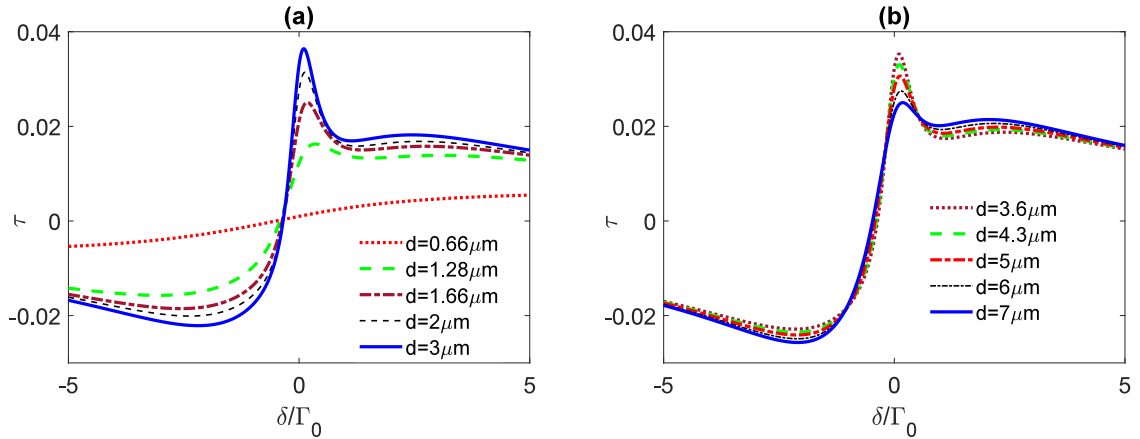


Fig. 9. (a) The variation of induced torque function τ (in units of s^{-1}) as a function of detuning δ (in units of γ) at the frequency 4 THz. Here, $\gamma' = 0$, $\omega_{32} = \Gamma_0$, $\lambda = 0$, $|\Omega_1| = 0.2\Gamma_0$, $|\Omega_2| = 0.1\Gamma_0$. (a) Shows the torque variation for distances $d = 0.66 \mu\text{m}$ (dotted line), $d = 1.28 \mu\text{m}$ (green dashed line), $d = 1.66 \mu\text{m}$ (dash-dotted line), $d = 2 \mu\text{m}$ (black dashed line), and $d = 3 \mu\text{m}$ (solid line), while (b) shows its variation for distances $d = 3.6 \mu\text{m}$ (dotted line), $d = 4.3 \mu\text{m}$ (dashed line), $d = 5 \mu\text{m}$ (red dash-dotted line), $d = 6 \mu\text{m}$ (black dash-dotted line) and $d = 7 \mu\text{m}$ (solid line). Note that Γ_0 is the decay rate in the vacuum.

We have also presented a remote distance control over the torque function when the double-V model QE is placed next to a planar surface of the topological insulator Bi_2Te_3 .

Such a double-V-model QE setup can be implemented experimentally in different atomic schemes having, for example, two $J = 0$ states

for the lower states, $|0\rangle$ and $|1\rangle$, and $M = \pm 1$ sublevels of a $J = 1$ state for excited states $|2\rangle$ and $|3\rangle$. The energy difference $\hbar\omega_{32}$ can be changed by a static magnetic field. In addition, the QE may be realized in hyperfine sublevels of D lines in alkali-metal atoms like ^{85}Rb and ^{87}Rb [63–65], or in dual CdSe/ZnS/CdSe quantum dots [63].

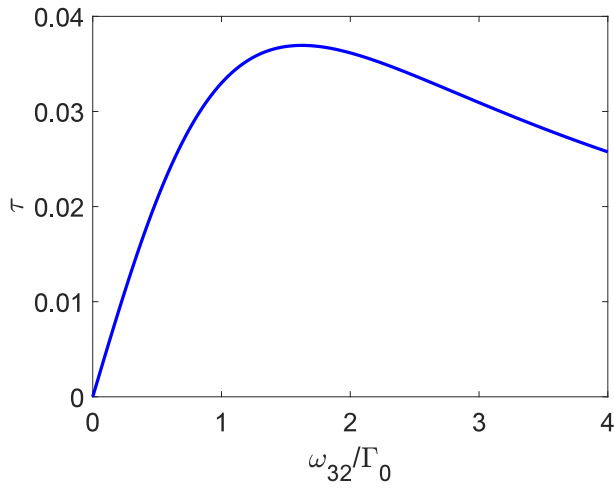


Fig. 10. The variation of induced torque function τ (in units of s^{-1}) as a function of splitting ω_{32} at the frequency 4 THz. Here, $\gamma' = 0$, $\delta = 0$, $\lambda = 0$, $|\Omega_1| = 0.2\Gamma_0$, $|\Omega_2| = 0.1\Gamma_0$ and $z = 3 \mu\text{m}$. Note that Γ_0 is the decay rate in the vacuum.

Our study makes several significant contributions to the field of optical manipulation of quantum emitters. Firstly, we demonstrated the use of quantum interference from spontaneous emission to manipulate and enhance light-induced torque, a technique not previously reported in literature. We derive analytical solutions for the steady-state density matrix equations for different initial states of the quantum system, demonstrating the significant impact of the initial state on torque variation and the possibility of generating absorption or lasing depending on the preparation of the system. Secondly, we presented a scenario in which the torque can be generated next to a photonic structure, allowing for remote distance control of this physical effect. These findings have important implications for the development of novel optical manipulation techniques and potential applications in quantum information processing and sensing.

CRediT authorship contribution statement

Hamid R. Hamed: Generated the idea for the study, Carried out the numerical and analytical investigations, Wrote the manuscript. **Julius Ruseckas:** Interpreted the results, Editing. **Vassilios Yannopoulos:** Interpreted the results, Editing. **Dimitrios Karoulanis:** Editing. **Emmanuel Paspalakis:** Collaborated with JR to design the theoretical methods, Editing.

Declaration of competing interest

The authors declare that they have no known competing financial interests or personal relationships that could have appeared to influence the work reported in this paper.

Data availability

Data will be made available on request.

Acknowledgments

This project has received funding from the Research Council of Lithuania (LMTLT), agreement No. S-PD-22-40.

Appendix

In this Appendix we provide the derivation of parameters γ and κ which as a result of the presence of the photonic structure have changed to Eqs. (40) and (41) [42,46,48,51,52,61]. Assuming that the orientation of the double-V QE dipoles are defined in terms of a nearby material surface, the spontaneous-emission rates are provided by

$$\gamma = \frac{\mu_0 \mu^2 \bar{\omega}^2}{2\hbar} \text{Im} [G_{\perp}(\mathbf{r}, \mathbf{r}; \bar{\omega}) + G_{\parallel}(\mathbf{r}, \mathbf{r}; \bar{\omega})] = \frac{1}{2}(\Gamma_{\perp} + \Gamma_{\parallel}), \quad (42)$$

$$\kappa = \frac{\mu_0 \mu^2 \bar{\omega}^2}{2\hbar} \text{Im} [G_{\perp}(\mathbf{r}, \mathbf{r}; \bar{\omega}) - G_{\parallel}(\mathbf{r}, \mathbf{r}; \bar{\omega})] = \frac{1}{2}(\Gamma_{\perp} - \Gamma_{\parallel}). \quad (43)$$

Here $G_{\perp}(\mathbf{r}, \mathbf{r}; \bar{\omega})$ and $G_{\parallel}(\mathbf{r}, \mathbf{r}; \bar{\omega})$ are the components of the electromagnetic Green's tensor of the surrounding environment, the symbol \perp and \parallel refers to a dipole oriented, respectively, normal (along the z axis) and parallel (along the x axis) to the surface of material, μ_0 is the permeability of vacuum and $\bar{\omega} = (\omega_3 + \omega_2)/2 - \omega_1$. The spontaneous emission rates, for an emitter oriented normal and parallel to the surface, are $\Gamma_{\perp,\parallel} = \mu_0 \mu^2 \bar{\omega}^2 \text{Im} [G_{\perp,\parallel}(\mathbf{r}, \mathbf{r}; \bar{\omega})] / \hbar$.

The electromagnetic Green's tensor providing the corresponding spontaneous emission rates Γ_{\perp} and Γ_{\parallel} is given by [52,72,73]

$$G_{ii'}^{PP}(\mathbf{r}, \mathbf{r}; \bar{\omega}) = g_{ii'}^{PP}(\mathbf{r}, \mathbf{r}; \omega) - \frac{i}{8\pi^2} \iint d^2\mathbf{k}_{\parallel} \frac{1}{c^2 K_z^+} v_{\mathbf{k}_{\parallel};i}(\mathbf{r}) \times \exp(-i\mathbf{K}^+ \cdot \mathbf{r}) \hat{\mathbf{e}}_i(\mathbf{K}^+), \quad (44)$$

with $v_{\mathbf{k}_{\parallel};i}(\mathbf{r}) = R^{PP'} \exp(-i\mathbf{K}^- \cdot \mathbf{r}) \hat{\mathbf{e}}_i(\mathbf{K}^-)$ and $\mathbf{K}^{\pm} = \{\mathbf{k}_{\parallel} \pm [q^2 - \mathbf{k}_{\parallel}^2]^{1/2}\}$ where \mathbf{k}_{\parallel} is the component of the wave vector, which is parallel to the material surface. $P, P' = E, H$ refer to the two independent polarization modes associated with the planar material surface. When $q^2 = \omega^2/c^2 < (k_{\parallel})^2$, the wave-vector \mathbf{K}^{\pm} defines an evanescent wave.

The term $g_{ii'}^{PP}(\mathbf{r}, \mathbf{r}; \omega)$ in Eq. (44) is the free-space Green's tensor and $\hat{\mathbf{e}}_i(\mathbf{K}^{\pm})$ is the polar unit vector normal to \mathbf{K}^{\pm} . Here also $R^{PP'}$ denotes the reflection matrix, which provides the reflected beam generated by the incidence of plane wave from above to the material slab [74]. Also, in Eq. (44) the terms corresponding to s-polarized waves (those containing components with the unit vector $\hat{\mathbf{e}}_i(\mathbf{K}^{\pm})$ normal to \mathbf{K}^{\pm}) make a trivial contribution to the total decay rates and thus have been neglected.

We assume then the slab of Bi_2Te_3 is thick enough so that we do not take into account finite-size effects. The dielectric function is modeled by [58,59,61]

$$\varepsilon_{\text{inp}}(\omega) = \sum_{j=\alpha,\beta,f} \frac{\omega_{pj}^2}{\omega_{0j}^2 - \omega^2 - i\gamma_j\omega}, \quad (45)$$

and it includes contributions from α and β transverse phonons, and free-charge carriers (f) arising from the bulk defects. The frequency parameters for the three terms appearing in Eq. (45) are taken from a fit to experimental data [75] on bulk Bi_2Te_3 and can be found in Table 1 of [59]. The subscripts appearing in the sum of Eq. (45) stem from contributions of α and β phonons, as well as from bulk free-charge carriers [75].

References

- [1] S.E. Harris, Electromagnetically induced transparency, *Phys. Today* 50 (1997) 36.
- [2] M. Fleischhauer, A. Imamoglu, J.P. Marangos, Electromagnetically induced transparency: Optics in coherent media, *Rev. Modern Phys.* 77 (2005) 633–673.
- [3] E. Paspalakis, P.L. Knight, Electromagnetically induced transparency and controlled group velocity in a multilevel system, *Phys. Rev. A* 66 (2002) 015802.
- [4] H.R. Gray, R.M. Whitley, C.R. Stroud, Coherent trapping of atomic populations, *Opt. Lett.* 3 (1978) 218–220.
- [5] G. Alzetta, A. Gozzini, L. Moi, G. Orriols, An experimental method for the observation of r.f. transitions and laser beat resonances in oriented Na vapour, *Nuovo Cimento B* 36 (1976) 5–20.
- [6] E. Arimondo, Coherent population trapping in laser spectroscopy, *Prog. Opt.* 35 (1996) 257.

- [7] K. Bergmann, H. Theuer, B.W. Shore, Coherent population transfer among quantum states of atoms and molecules, *Rev. Modern Phys.* 70 (1998) 1003–1025.
- [8] N.V. Vitanov, A.A. Rangelov, B.W. Shore, K. Bergmann, Stimulated Raman adiabatic passage in physics, chemistry, and beyond, *Rev. Modern Phys.* 89 (2017) 015006.
- [9] J. Mompart, R. Corbalan, Lasing without inversion, *J. Opt. B: Quantum Semiclass. Opt.* 2 (2000) R7–R24.
- [10] A.A. Svidzinsky, L. Yuan, M.O. Scully, Transient lasing without inversion, *New J. Phys.* 15 (2013) 053044.
- [11] G. Juzeliūnas, H.J. Carmichael, Systematic formulation of slow polaritons in atomic gases, *Phys. Rev. A* 65 (2002) 021601(R).
- [12] G. Juzeliūnas, P. Öhberg, Slow light in degenerate Fermi gases, *Phys. Rev. Lett.* 93 (2004) 033602.
- [13] S.E. Harris, J.E. Field, A. Imamoglu, Nonlinear optical processes using electromagnetically induced transparency, *Phys. Rev. Lett.* 64 (1990) 1107–1110.
- [14] H. Wang, D. Goorskey, M. Xiao, Enhanced Kerr nonlinearity via atomic coherence in a three-level atomic system, *Phys. Rev. Lett.* 87 (2001) 073601.
- [15] A.S. Zibrov, A.B. Matsko, O. Kocharovskaya, Y.V. Rostovtsev, G.R. Welch, M.O. Scully, Transporting and time reversing light via atomic coherence, *Phys. Rev. Lett.* 88 (2002) 103601.
- [16] D.A. Braje, V. Balić, G.Y. Yin, S.E. Harris, Low-light-level nonlinear optics with slow light, *Phys. Rev. A* 68 (2003) 041801.
- [17] L. Allen, M.J. Padgett, M. Babiker, IV the orbital angular momentum of light, *Prog. Opt.* 39 (1999) 291–372.
- [18] L. Allen, M.W. Beijersbergen, R.J.C. Spreeuw, J.P. Woerdman, Orbital angular momentum of light and the transformation of Laguerre–Gaussian laser modes, *Phys. Rev. A* 45 (1992) 8185–8189.
- [19] N.R. Heckenberg, R. McDuff, C.P. Smith, A.G. White, Generation of optical phase singularities by computer-generated holograms, *Opt. Lett.* 17 (1992) 221–223.
- [20] I.G. Mariyenko, J. Strohaber, C.J.G.J. Uiterwaal, Creation of optical vortices in femtosecond pulses, *Opt. Express* 13 (2005) 7599–7608.
- [21] J. Ruseckas, G. Juzeliūnas, P. Öhberg, S.M. Barnett, Polarization rotation of slow light with orbital angular momentum in ultracold atomic gases, *Phys. Rev. A* 76 (2007) 053822.
- [22] Q.-F. Chen, B.-S. Shi, Y.-S. Zhang, G.-C. Guo, Entanglement of the orbital angular momentum states of the photon pairs generated in a hot atomic ensemble, *Phys. Rev. A* 78 (2008) 053810.
- [23] N. Radwell, T.W. Clark, B. Piccirillo, S.M. Barnett, S. Franke-Arnold, Spatially dependent electromagnetically induced transparency, *Phys. Rev. Lett.* 114 (2015) 123603.
- [24] H.R. Hamedí, V. Kudriasov, J. Ruseckas, G. Juzeliūnas, Azimuthal modulation of electromagnetically induced transparency using structured light, *Opt. Express* 26 (2018) 28249–28262.
- [25] H.R. Hamedí, G. Zlabys, V. Ahufinger, T. Halfmann, J. Mompart, G. Juzeliūnas, Spatially strongly confined atomic excitation via a two dimensional stimulated Raman adiabatic passage, *Opt. Express* 30 (2022) 13915–13930.
- [26] H.R. Hamedí, E. Paspalakis, G. Žlabys, G. Juzeliūnas, J. Ruseckas, Complete energy conversion between light beams carrying orbital angular momentum using coherent population trapping for a coherently driven double- Λ atom-light-coupling scheme, *Phys. Rev. A* 100 (2019) 023811.
- [27] N. Jia, J. Qian, T. Kirova, G. Juzeliūnas, H.R. Hamedí, Ultraprecise rydberg atomic localization using optical vortices, *Opt. Express* 28 (2020) 36936–36952.
- [28] F. Castellucci, T.W. Clark, A. Selyem, J. Wang, S. Franke-Arnold, Atomic compass: Detecting 3D magnetic field alignment with vector vortex light, *Phys. Rev. Lett.* 127 (2021) 233202.
- [29] J.W.R. Tabosa, D.V. Petrov, Optical pumping of orbital angular momentum of light in cold cesium atoms, *Phys. Rev. Lett.* 83 (1999) 4967–4970.
- [30] H. He, M.E.J. Friese, N.R. Heckenberg, H. Rubinsztein-Dunlop, Direct observation of transfer of angular momentum to absorptive particles from a laser beam with a phase singularity, *Phys. Rev. Lett.* 75 (1995) 826–829.
- [31] M.E.J. Friese, J. Enger, H. Rubinsztein-Dunlop, N.R. Heckenberg, Optical angular-momentum transfer to trapped absorbing particles, *Phys. Rev. A* 54 (1996) 1593–1596.
- [32] M. Babiker, W.L. Power, L. Allen, Light-induced torque on moving atoms, *Phys. Rev. Lett.* 73 (1994) 1239–1242.
- [33] V. Garcés-Chávez, D. McGloin, M.J. Padgett, W. Dultz, H. Schmitzer, K. Dholakia, Observation of the transfer of the local angular momentum density of a multiringed light beam to an optically trapped particle, *Phys. Rev. Lett.* 91 (2003) 093602.
- [34] M.F. Andersen, C. Ryu, P. Clade, V. Natarajan, A. Vaziri, K. Helmerson, W.D. Phillips, Quantized rotation of atoms from photons with orbital angular momentum, *Phys. Rev. Lett.* 97 (2006) 170406.
- [35] C.M. Herne, K.M. Capuzzi, E. Sobel, R.T. Kropas, Rotation of large asymmetrical absorbing objects by Laguerre–Gauss beams, *Opt. Lett.* 40 (2015) 4026–4029.
- [36] V.E. Lembessis, M. Babiker, Light-induced torque for the generation of persistent current flow in atomic gas Bose–Einstein condensates, *Phys. Rev. A* 82 (2010) 051402.
- [37] K.T. Kapale, J.P. Dowling, Vortex phase qubit: Generating arbitrary, counterrotating, coherent superpositions in Bose–Einstein condensates via optical angular momentum beams, *Phys. Rev. Lett.* 95 (2005) 173601.
- [38] A. Mair, A. Vaziri, G. Weihs, A. Zeilinger, Entanglement of the orbital angular momentum states of photons, *Nature* 412 (2001) 313–316.
- [39] M.O. Scully, S.-Y. Zhu, A. Gavrielides, Degenerate quantum-beat laser: Lasing without inversion and inversion without lasing, *Phys. Rev. Lett.* 62 (1989) 2813–2816.
- [40] P. Zhou, S. Swain, Quantum interference in probe absorption: Narrow resonances, transparency, and gain without population inversion, *Phys. Rev. Lett.* 78 (1997) 832.
- [41] E. Paspalakis, S.-Q. Gong, P. L.Knight, Spontaneous emission-induced coherent effects in absorption and dispersion of a V-type three-level atom, *Opt. Commun.* 152 (1998) 293–298.
- [42] P.K. Jha, X. Ni, C. Wu, Y. Wang, X. Zhang, Metasurface-enabled remote quantum interference, *Phys. Rev. Lett.* 115 (2015) 025501.
- [43] P.K. Jha, N. Shitrit, X. Ren, Y. Wang, X. Zhang, Spontaneous exciton valley coherence in transition metal dichalcogenide monolayers interfaced with an anisotropic metasurface, *Phys. Rev. Lett.* 121 (2018) 116102.
- [44] G.S. Agarwal, A.K. Patnaik, Vacuum-induced coherences in radiatively coupled multilevel systems, *Phys. Rev. A* 63 (2001) 043805.
- [45] G.-x. Li, F.-l. Li, S.-y. Zhu, Quantum interference between decay channels of a three-level atom in a multilayer dielectric medium, *Phys. Rev. A* 64 (2001) 013819.
- [46] Y. Yang, J. Xu, H. Chen, S. Zhu, Quantum interference enhancement with left-handed materials, *Phys. Rev. Lett.* 100 (2008) 043601.
- [47] L. Sun, C. Jiang, Quantum interference in a single anisotropic quantum dot near hyperbolic metamaterials, *Opt. Express* 24 (2016) 7719–7727.
- [48] S. Hughes, G.S. Agarwal, Anisotropy-induced quantum interference and population trapping between orthogonal quantum dot exciton states in semiconductor cavity systems, *Phys. Rev. Lett.* 118 (2017) 063601.
- [49] F. Le Kien, V.I. Balykin, K. Hakuta, Light-induced force and torque on an atom outside a nanofiber, *Phys. Rev. A* 74 (2006) 033412.
- [50] G.S. Agarwal, Anisotropic vacuum-induced interference in decay channels, *Phys. Rev. Lett.* 84 (2000) 5500–5503.
- [51] G.-x. Li, J. Evers, C.H. Keitel, Spontaneous emission interference in negative-refractive-index waveguides, *Phys. Rev. B* 80 (2009) 045102.
- [52] V. Yannopapas, E. Paspalakis, N.V. Vitanov, Plasmon-induced enhancement of quantum interference near metallic nanostructures, *Phys. Rev. Lett.* 103 (2009) 063602.
- [53] I. Thanopoulos, V. Yannopapas, E. Paspalakis, Non-Markovian dynamics in plasmon-induced spontaneous emission interference, *Phys. Rev. B* 95 (2017) 075412.
- [54] V. Karanikolas, E. Paspalakis, Plasmon-induced quantum interference near carbon nanostructures, *J. Phys. Chem. C* 122 (2018) 14788.
- [55] I. Thanopoulos, V. Karanikolas, E. Paspalakis, Non-Markovian spontaneous emission interference near a MoS₂ nanodisk, *Opt. Lett.* 44 (2019) 3510–3513.
- [56] X. Zeng, Z. Li, G.-Q. Ge, M.S. Zubairy, Quantum interference near graphene layers: Observing the surface plasmons with transverse electric polarization, *Phys. Rev. A* 99 (2019) 043811.
- [57] N.P. Butch, K. Kirshenbaum, P. Syers, A.B. Sushkov, G.S. Jenkins, H.D. Drew, J. Paglione, Strong surface scattering in ultrahigh-mobility Bi₂Se₃ topological insulator crystals, *Phys. Rev. B* 81 (2010) 241301.
- [58] G. Siroki, D.K.K. Lee, P.D. Haynes, V. Giannini, Single-electron induced surface plasmons on a topological nanoparticle, *Nature Commun.* 7 (2016) 12375.
- [59] M.S. Rider, M. Sokolikova, S.M. Hanham, M.N. Cia, P. D.Haynes, D.K.K. Lee, M. Daniele, M.C. Guidi, C. Mattevi, S. Lupi, V. Giannini, Experimental signature of a topological quantum dot, *Nanoscale* 12 (2020) 22817–22825.
- [60] D. Karaoulanis, V. Yannopapas, Quantum interference of spontaneous-emission channels near the surface of Bi₂Se₃, *Internat. J. Modern Phys. B* 35 (2021) 2150154.
- [61] D. Karaoulanis, E. Paspalakis, V. Yannopapas, Quantum interference near bismuth-chalcogenidemicrostructures, *J. Opt. Soc. Amer. B* 38 (2021) 3301–3308.
- [62] G.D. Chatzidakis, V. Yannopapas, Strong electromagnetic coupling in dimers of topological-insulator nanoparticles and quantum emitters, *Phys. Rev. B* 101 (2020) 165410.
- [63] L. Wang, Y. Gu, H. Chen, J.-Y. Zhang, Y. Cui, B.D. Gerardot, Q. Gong, Polarized linewidth-controllable double-trapping electromagnetically induced transparency spectra in a resonant plasmon nanocavity, *Sci. Rep.* 3 (2013) 2879.
- [64] M. Sukharev, S.A. Malinovskaya, Stimulated Raman adiabatic passage as a route to achieving optical control in plasmonics, *Phys. Rev. A* 86 (2012) 043406.
- [65] Y. Gu, L. Wang, P. Ren, J. Zhang, T. Zhang, O.J.F. Martin, Q. Gong, Surface-plasmon-induced modification on the spontaneous emission spectrum via subwavelength-confined anisotropic Purcell factor, *Nano Lett.* 12 (2012) 2488–2493.
- [66] M. Scully, M. Zubairy, *Quantum Optics*, Cambridge University Press, Cambridge, 1997.
- [67] W.-H. Xu, J.-H. Wu, J.-Y. Gao, Gain with and without population inversion via vacuum-induced coherence in a V-type atom without external coherent driving, *J. Phys. B: At. Mol. Opt. Phys.* 39 (2006) 1461–1471.
- [68] S. Evangelou, V. Yannopapas, E. Paspalakis, Transparency and slow light in a four-level quantum system near a plasmonic nanostructure, *Phys. Rev. A* 86 (2012) 053811.

- [69] E. Paspalakis, S. Evangelou, V. Yannopoulos, A.F. Terzis, Phase-dependent optical effects in a four-level quantum system near a plasmonic nanostructure, *Phys. Rev. A* 88 (2013) 053832.
- [70] H.R. Hamed, V. Yannopoulos, G. Juzeliūnas, E. Paspalakis, Coherent optical effects in a three-level quantum emitter near a periodic plasmonic nanostructure, *Phys. Rev. B* 106 (2022) 035419.
- [71] M. Kiffner, M. Macovei, J. Evers, C.H. Keitel, Chapter 3 - vacuum-induced processes in multilevel atoms, *Prog. Opt.* 55 (2010) 85–197.
- [72] R. Sainidou, N. Stefanou, A. Modinos, Green's function formalism for phononic crystals, *Phys. Rev. B* 69 (2004) 064301.
- [73] V. Yannopoulos, N.V. Vitanov, Electromagnetic Green's tensor and local density of states calculations for collections of spherical scatterers, *Phys. Rev. B* 75 (2007) 115124.
- [74] N. Stefanou, V. Yannopoulos, A. Modinos, Heterostructures of photonic crystals: frequency bands and transmission coefficients, *Comput. Phys. Comm.* 113 (1998) 49–77.
- [75] A. Dubroka, O. Caha, M. Hronček, P. Friš, M. Orlita, V. Holý, H. Steiner, G. Bauer, G. Springholz, J. Humlíček, Interband absorption edge in the topological insulators $\text{Bi}_2(\text{Te}_{1-x}\text{Se}_x)_3$, *Phys. Rev. B* 96 (2017) 235202.